COMMUNICATION

pubs.acs.org/Biomac

Porphyrin-Cross-Linked Hydrogel for Fluorescence-Guided Monitoring and Surgical Resection

Jonathan F. Lovell,[†,∥,#] Aron Roxin,[‡,∥] Kenneth K. Ng,[†,∥] Qiaochu Qi,[§,∥] Jesse D. McMullen,[§,∥] Ralph S. DaCosta,[§,∥] and Gang Zheng[†,§,∥,*]

[†]Institute of Biomaterials and Biomedical Engineering, [‡]Department of Pharmaceutical Sciences, [§]Department of Medical Biophysics, and [∥]Ontario Cancer Institute, University of Toronto, ON, M5G 1L7, Canada

[#]Department of Biomedical Engineering, University at Buffalo, The State University of New York, Buffalo, New York 14260, United States

Supporting Information

ABSTRACT: We demonstrate that porphyrins can be used as efficient cross-linkers to generate a new class of hydrogels with enabling optical properties. Tetracarboxylic acid porphyrins reacted with PEG diamines to form a condensation polyamide in a range of appropriate conditions, with respect to reaction time, diisopropylethylamine initiator concentration, porphyrin-to-PEG ratio, porphyrin concentration, and PEG size. The network structure of the hydrogel maintained a porphyrin spacing that prevented excessive fluorescence self-quenching despite high porphyrin density. The near-infrared properties readily enabled low background, noninvasive fluorescence monitoring of the implanted hydrogel in vivo, as well as its image-guided surgical removal in real time using a low-cost fluorescence camera prototype. Emission could be tuned by incorporating copper metalloporphyrins into the network. The approach of creating hydrogels using cross-linking porphyrin comonomers creates opportunities for new polymer designs with strong optical character.

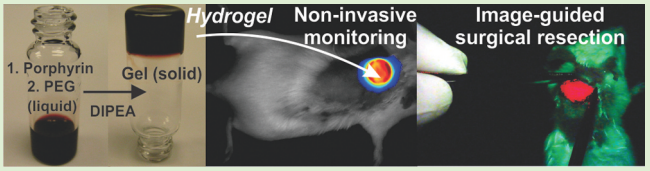

INTRODUCTION

Hydrogels are hydrophilic and absorbent 3-D polymers that have emerged as useful tools for applications in drug delivery, tissue engineering, contact lenses, and implants.[1−3] Implants can be powerful drug delivery systems, with the capability of releasing drugs over several years (e.g., for birth control).[4] Noninvasive methods to easily monitor implant stability could benefit testing and design of the material. Moreover, when implant removal is required, noninvasive methods to locate the implant and even guide the surgical removal of the implant could be useful. Fluorescence imaging is an attractive technique for noninvasive monitoring and image-guided surgery, but so far, there have been a few examples of these applications with respect to implantable hydrogels. Hydrogels can be formed from a range of both natural and synthetic polymers.[5] Even therapeutic agents themselves can be used to form hydrogels.[6] Among synthetic constituents, polyethylene glycol (PEG) is an attractive monomer for hydrogels, given its favorable availability, biocompatibilty, and swelling capacity.[7,8] PEG hydrogels have been formed through a multitude of polymerization routes including photoinduced radical polymerization, ring-opening polymerization, click chemistry, and star polymers, among others.[9−14] Porphyrins, which have strong optical absorption, have been explored as cargo for hydrogels; however, loading efficiency has been limited, and passively loaded porphyrins eventually migrate out of the gel.[15−18] Porphyrins have also been characterized extensively in thin films; however, these are generally not robust enough for in vivo applications. Here we use porphyrins as cross-linkers using a rapid stepwise condensation copolymerization reaction between PEG spacers with amine functionality of 2 and porphyrins with acid functionality of 4. Thus, porphyrin-cross-linked hydrogels have stable, alternating porphyrin and PEG subunits that generated substantial near-infrared optical character, permitting long-term, noninvasive fluorescence monitoring and image-guided surgical resection in vivo. This approach is unique in that porphyrins are not passively conjugated to the system but rather anchor and drive the formation of the 3-D network. Because the porphyrins alternate with PEG spacers, a homogeneous spatial density of porphyrins was achieved. While maintaining a high porphyrin density, this spatial pattern prevented extensive porphyrin aggregation and fluorescence self-quenching, which can occur during porphyrin conjugation to polymers (a phenomenon that is sometimes used to design activatable photosensitizers and porphyrin-based nanoparticles).[19]

RESULTS AND DISCUSSION

To generate the hydrogel, we used *meso*-tetrakis(4-carboxyphenyl) porphine (mTCPP) and a diamine-functionalized PEG spacer (Figure 1a). We hypothesized that upon amide bond formation, the PEG spacers and porphyrins would form an interconnected 3-D matrix, as shown schematically in Figure 1b. mTCPP, PEG-diamine, and the acid activator HBTU were combined in

Received: June 10, 2011
Revised: July 19, 2011

   dx.doi.org/10.1021/bm200784s | *Biomacromolecules* XXXX, XXX, 000–000

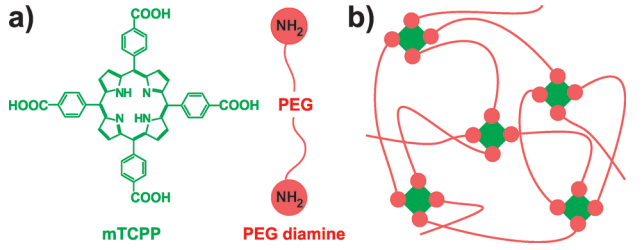

Figure 1. Porphyrin-cross-linked hydrogels. (a) Structures of mTCPP (green) and PEG diamine (red). (b) Schematic of the hydrogel.

dimethylformamide (DMF) in a 1:2:4 ratio. These ratios were equimolar with respect to the functionality of each component because each of the four acid groups of mTCPP could be activated with one HBTU and react with each of the two amine groups on the connecting PEG linkers.

Upon addition of diisopropylethylamine (DIPEA), the activated acid groups of mTCPP reacted with the amine groups of the PEG in situ (Figure 2a). This reaction occurred rapidly, and complete gelation was apparent in seconds as the solution converted to a thick solid gel that remained fully insoluble when more solvent was added. Polymerization efficiency was assessed by quantifying the total amount of unincorporated mTCPP that washed out of a gel piece. Over 97% of the porphyrin polymerized within 10 s of adding DIPEA to initiate the polymerization (Figure 2b). At 5 s, gelation was markedly reduced, and almost no gelation occurred 1 s after DIPEA addition. The infrared spectra of the polymerized gel showed complete conversion of the acid groups of mTCPP into amides (Figure 1 of the Supporting Information). Thus, DIPEA activation of the porphyrin acid groups and subsequent polymerization occurred in situ rapidly with high efficiency. We next examined how the amount of DIPEA added affected polymerization. Full polymerization was observed with ≥0.2% DIPEA in the gel solution, which corresponded to an approximately 2:1 molar ratio of DIPEA/mTCPP (Figure 2c). Besides the activating conditions, the ratio of PEG diamine to mTCPP played a role in polymerization efficiency. As shown in Figure 2d, an optimal ratio occurred at 1:2 mTCPP-to-PEG ratio, corresponding to four carboxylic acid groups for each two amine groups on the PEG linkers. This represents an equimolar functional group ratio. Polymerization was then assessed as a function of porphyrin concentration (Figure 2e). Below 2 mM porphyrin, there was a rapid decrease in hydrogelation efficiency, demonstrating that polymerization was sensitive to concentration of the comonomers. As the porphyrin and PEG density increased, less water could be absorbed into the hydrogels (Figure 2f). Gels polymerized using 2 mM porphyrin in the starting solution had a final water swelling ratio of 7000%, whereas gels polymerized with 5 mM porphyrin concentration had a water swelling ratio of 3000%. As expected, mTCPP density (which was estimated based on the mass of the hydrogels and using the density of water) was inversely proportional to water swelling. Starting porphyrin concentration of 2 mM generated an mTCPP density of $\sim 5 \times 10^{11}$ mTCPP molecules per cubic centimeter of swollen gel. When the starting porphyrin concentration was increased to 5 mM, mTCPP density increased to $>16 \times 10^{11}$ mTCPP molecules per cubic centimeter of swollen gel. Given the sensitive polymerization conditions, the effect of different length PEG diamine spacers was investigated. Porphyrin-anchored hydrogels polymerized effectively using the longer

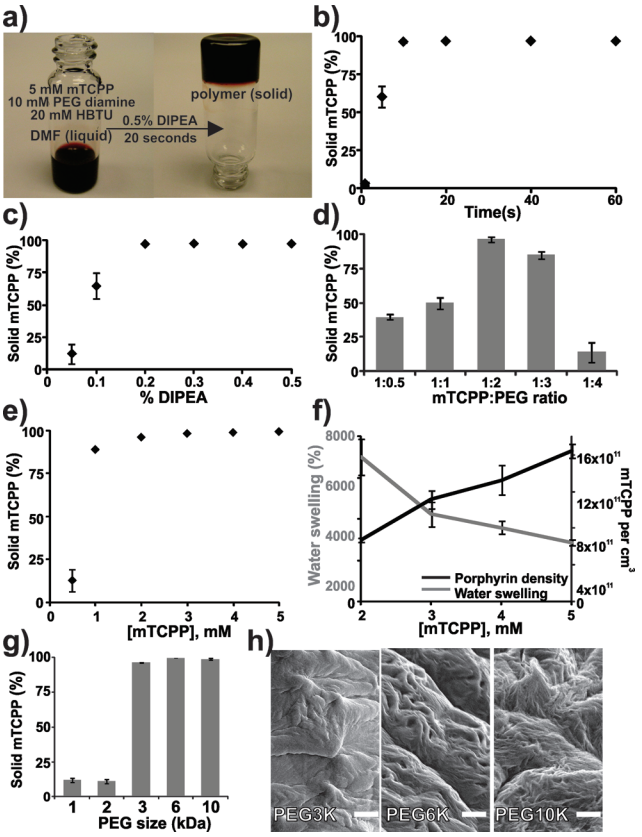

Figure 2. Characterization of hydrogel formation. (a) Photographs of polymerization. Polymerization efficiencies, measured by % of mTCPP covalently incorporated into solid polymer as function of (b) time after DIPEA addition. (c) DIPEA concentration. (d) mTCPP to PEG molar ratio. (e) mTCPP concentration. (f) Water swelling and porphyrin density for varying starting porphyrin concentrations. (g) Polymerization efficiency using PEG of indicated size. (h) Corresponding scanning electron micrographs with 2 μm scale bar shown. Unless otherwise noted, gels were formed with a mTCPP/PEG(6 kDa)/HBTU ratio of 1:2:4. Error bars show mean ± SD (n = 3).

10, 6, and 3 kDa PEG diamine linkers but not with the shorter 1 and 2 kDa linkers (Figure 2g). Because the total amine concentration was constant with the different length PEG spacers, the lack of full polymerization using shorter linkers suggests that gelation required specific intermolecular spacing between functional groups. The different length spacers generated hydrogels with distinct surface character (Figure 2h).

As a typical tetrapyrrolic porphyrin, mTCPP has a major Soret band absorbance around 405 nm and weak absorbance in the red-shifted Q-bands. However, the Q-band absorbance is relevant for in vivo imaging because shorter wavelength light is rapidly attenuated in tissues. Despite the relatively low Q-band absorption of mTCPP, the dense mTCPP spacing of the porphyrin-anchored gels conferred strong absorption between 500 and 700 nm (Figure 3a). The gel was highly fluorescent, and the emission had two primary peaks at 660 and 710 nm, with the emission peaks shifting slightly depending on the environment of the gel (Figure 3b, which shows the emission spectra in both the aqueous in vivo environment and following polymerization in DMF). The mTCPP remained stably incorporated in the hydrogel when incubated at 37 °C in buffered saline, whereas mTCPP passively incorporated in hydrogels of varying agarose

dx.doi.org/10.1021/bm200784s |*Biomacromolecules* XXXX, XXX, 000–000

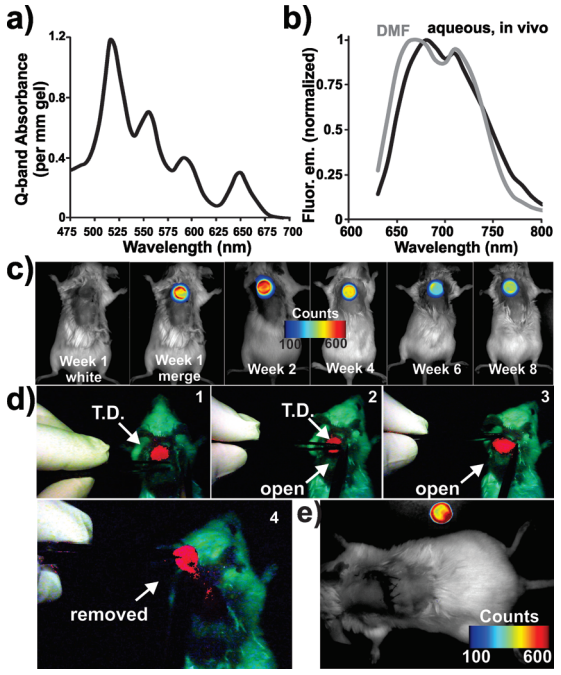

Figure 3. Noninvasive monitoring and image-guided surgical resection of porphyrin-cross-linked hydrogel. (a) Q-band absorption spectrum of a section of the hydrogel, 1 mm in depth. (b) Fluorescence emission spectra of the hydrogel in DMF following polymerization and in vivo. (c) Fluorescence images of a mouse with the hydrogel implanted subcutaneously and monitored noninvasively. (d) Screen captures from a fluorescence camera used to guide fluorescently the surgical removal of the hydrogel in real time. Fluorescence was readily apparent transdermally (T.D.) or through the open incision, as indicated. (e) Fluorescence image of the mouse and hydrogel following image-guided surgical hydrogel resection and incision suturing.

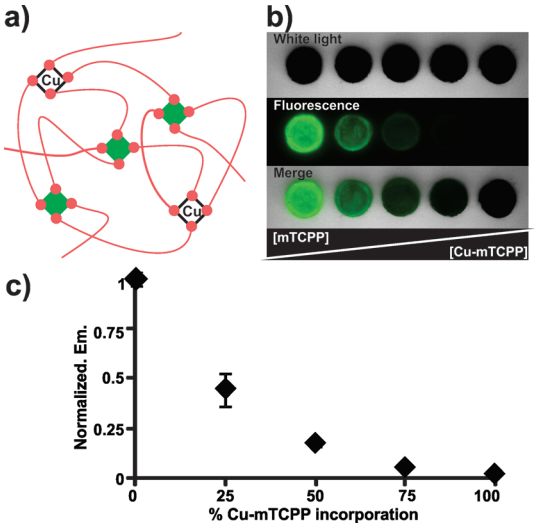

Figure 4. Modulation of optical properties using metal substituted porphyrins. (a) Schematic of Cu-mTCPP (nonfluorescent) in mTCPP hydrogel. (b) Optical imaging of water-equilibrated mTCPP hydrogels containing 0, 25, 50, 75, and 100% Cu-mTCPP. (c) Quantification of gel fluorescence intensity. Error bars show mean ± SD (n = 3).

concentration leaked out over a period of 1 week (Figure 2 of the Supporting Information). The near-infrared character permitted the noninvasive fluorescence monitoring of a subcutaneously implanted hydrogel in a mouse in vivo. Over a 2 month period following implantation, the mouse displayed no adverse effects or behavior, demonstrating the biocompatibility of the gel. Using an optical imaging system, the fluorescence signal could be distinguished in vivo with essentially no background using only a 40 ms camera exposure. Fluorescence imaging was performed weekly to visualize noninvasively where the gel was located and whether hydrogel degradation or photobleaching occurred (Figure 3c). The appearance of a brighter outer ring in gel was caused by a slightly uneven spatial distribution of the prepolymerized solution in the casting mold. During the monitoring period, noninvasive fluorescence imaging demonstrated that the porphyrin-anchored hydrogel maintained its form and placement in vivo. The consistent fluorescence levels suggested there was minimal fluorescence bleaching or hydrogel degradation during that time. Therefore, the porphyrin-anchored hydrogel permitted the noninvasive assessment of position, shape, and degradation. We next used a fluorescence camera to guide the surgical removal of the gels. This camera was equipped with 405 nm excitation light emitting diodes and a 600 nm long-pass filter and functioned in real-time (no long integrations) and was based on a standard digital camera lacking a cooled CCD. The gel was readily viewable using the camera. For better clarity, the images shown in Figure 3d were uniformly enhanced based on the red channel of the images, and in the future, such an image processing algorithm could be directly integrated into the camera hardware or software. A movie of the surgical procedure is available in the supporting materials. Using the display screen of the camera, surgery was performed and was greatly facilitated because the position of the gel was known at all times using the images on the camera. Following surgical resection, the incisions were sutured closed, and the mouse was imaged again using the standard imager (Figure 3e). No residual fluorescence was detected in the mouse, and the bright hydrogel fluorescence of the removed gel was easily recognized.

When mTCPP chelates copper, fluorescence generation is quenched. We hypothesized that copper porphyrin could be stably titrated into the hydrogel, resulting in an organometallic framework with modified fluorescence properties. Figure 4a shows a schematic depiction of a hydrogel in which some of the mTCPP porphyrin anchors are substituted with copper-chelated mTCPP (Cu-mTCPP). Using a slightly modified polymerization protocol, a series of hydrogels were formed with increasing amount of Cu-mTCPP and examined using fluorescence imaging (Figure 4b). The hydrogels formed from only mTCPP were fluorescent, but because Cu-mTCPP was titrated into the gel, the fluorescence generation was attenuated. Quantification of the fluorescence intensities of the gels revealed a nonlinear relationship between the amount of quenching and the Cu-mTCPP concentration, suggesting that Cu-mTCPP could dynamically quench other mTCPP moieties in the 3-D network (Figure 4c). The Cu-mTCPP hydrogels were biocompatible and maintained their fluorescence quenching in vivo (Figure 3 of the Supporting Information). Tuning of hydrogel properties using metal chelation could have a variety of applications. For instance, because it is fluorescently quenched, near-infrared light energy absorbed by the Cu-mTCPP network would be expected to be more efficiently converted to heat, which could have future applications for heat-activated drug release. Whereas the porphyrin-cross-linked hydrogel fluorescence was used to monitor location, shape, and degradation and to guide surgery, future

dx.doi.org/10.1021/bm200784s |*Biomacromolecules* XXXX, XXX, 000–000

work could use the optical properties of the gel for other interesting applications. For instance, if certain drugs affected the fluorescence properties of the hydrogel, they could be used to monitor drug release noninvasively. Alternatively, the hydrogel could be used to measure oxygen concentration by using platinum porphyrins, which are known to be effective oxygen sensors.[20] Apart from optical applications, other potential uses include using the metalloporphyrin hydrogel for catalytic purposes because metalloporphyrins are known to be excellent oxidation catalysts.[21]

In summary, we have used porphyrins to generate a new class of optically active hydrogels. mTCPP was as an effective crosslinking comonomer for PEG diamines, which rapidly formed stable, condensation polyamide hydrogels. The high porphyrin density and near-infrared character permitted noninvasive monitoring, and the implanted hydrogels were stable in mice with minimal change in position, shape, or significant bleaching or degradation over a 2 month period. The high fluorescence of the hydrogel also permitted real-time, image-guided surgical resection of the hydrogel in vivo using an affordable prototype fluorescence camera. Optical properties were modulated when nonfluorescent metalloporphyrins were used in the gel. The approach of using porphyrins as polymer comonomers could be extended to generate new optical polymers using different types of linkers.

■ ASSOCIATED CONTENT

Supporting Information. Full experimental methods, FTIR spectra, and a video clip demonstrating the image-guided surgical hydrogel resection. This material is available free of charge via the Internet at http://pubs.acs.org.

■ AUTHOR INFORMATION

Corresponding Author
*E-mail: gzheng@uhnres.utoronto.ca.

■ ACKNOWLEDGMENT

This work was supported by the Canadian Cancer Society, the Natural Sciences and Engineering Research Council of Canada, the Canadian Foundation of Innovation, the Canadian Institute of Health Research, and the Joey and Toby Tanenbaum/Brazilian Ball Chair in Prostate Cancer Research. We thank Prof. Mitch Winnik for valuable discussion about polymerization principles, and Meena Purohit and Prof. Lakshimi Kotra for assistance with FTIR measurements.

■ REFERENCES

(1) Hoare, T. R.; Kohane, D. S. *Polymer* **2008**, *49*, 1993–2007.
(2) Lee, K. Y.; Mooney, D. J. *Chem. Rev.* **2001**, *101*, 1869–1880.
(3) Kopecek, J. *J. Polym. Sci., Part A: Polym. Chem.* **2009**, *47* 5929–5946.
(4) Dash, A. K.; Cudworth, G. C., II *J. Pharmacol. Toxicol. Methods* **1998**, *40*, 1–12.
(5) Hoffman, A. S. *Adv. Drug Delivery Rev.* **2002**, *54*, 3–12.
(6) Zhao, F.; Ma, M. L.; Xu, B. *Chem. Soc. Rev.* **2009**, *38*, 883.
(7) Lin, C.-C.; Anseth, K. S. *Pharm. Res.* **2008**, *26*, 631–643.
(8) Harris, J. M.; Chess, R. B. *Nat. Rev. Drug Discovery* **2003**, *2* 214–221.
(9) Nederberg, F.; Trang, V.; Pratt, R. C.; Mason, A. F.; Frank, C. W.; Waymouth, R. M.; Hedrick, J. L. *Biomacromolecules* **2007**, *8*, 3294–3297.
(10) Malkoch, M.; Vestberg, R.; Gupta, N.; Mespouille, L.; Dubois, P.; Mason, A. F.; Hedrick, J. L.; Liao, Q.; Frank, C. W.; Kingsbury, K.; Hawker, C. J. *Chem. Commun.* **2006**, 2774–2776.
(11) Peppas, N. A.; Keys, K. B.; Torres-Lugo, M.; Lowman, A. M. *J. Controlled Release* **1999**, *62*, 81–87.
(12) Fairbanks, B. D.; Schwartz, M. P.; Bowman, C. N.; Anseth, K. S. *Biomaterials* **2009**, *30*, 6702–6707.
(13) Hennink, W. E.; van Nostrum, C. F. *Adv. Drug Delivery Rev.* **2002**, *54*, 13–36.
(14) Lutolf, M. P.; Hubbell, J. A. *Biomacromolecules* **2003**, *4*, 713–722.
(15) Brady, C.; Bell, S. E. J.; Parsons, C.; Gorman, S. P.; Jones, D. S.; McCoy, C. P. *J. Phys. Chem. B* **2007**, *111*, 527–534.
(16) Ng, L.-T.; Swami, S.; Gordon-Thomson, C. *Radiat. Phys. Chem.* **2006**, *75*, 604–612.
(17) Li, Y.-z.; He, N.; Ci, Y.-x. *Analyst* **1998**, *123*, 359–364.
(18) Gao, D.; Xu, H.; Philbert, M. A.; Kopelman, R. *Angew. Chem., Int. Ed.* **2007**, *46*, 2224–2227.
(19) (a) Lovell, J. F.; Liu, T. W. B.; Chen, J.; Zheng, G. *Chem. Rev.* **2010**, *110*, 2839–2857. (b) Lovell, J. F.; Jin, C. S.; Huynh, E.; Jin, H.; Kim, C.; Rubinstein, J. L.; Chan, W. C. W.; Cao, W.; Wang, L. V.; Zheng, G. *Nat. Materials.* **2011**, *10*, 324–332.
(20) Lee, S.-K.; Okura, I. *Anal. Commun.* **1997**, *34*, 185–188.
(21) Meunier, B. *Chem. Rev.* **1992**, *92*, 1411–1456.